

1           **Full-coverage 1 km daily ambient PM<sub>2.5</sub> and O<sub>3</sub> concentrations of China in**  
2                           **2005-2017 based on multi-variable random forest model**

3  
4   Runmei Ma<sup>1#</sup>, Jie Ban<sup>1#</sup>, Qing Wang<sup>1#</sup>, Yayi Zhang<sup>1</sup>, Yang Yang<sup>2</sup>, Shenshen Li<sup>3</sup>,  
5   Wenjiao Shi<sup>4,5</sup>, Zhen Zhou<sup>1,6</sup>, Jiawei Zang<sup>1,6</sup>, Tiantian Li<sup>1\*</sup>

6  
7   <sup>1</sup> China CDC Key Laboratory of Environment and Population Health, National Institute of  
8   Environmental Health, Chinese Center for Disease Control and Prevention, Beijing, 100021,  
9   China

10   <sup>2</sup> Institute of Urban Meteorology, China Meteorological Administration, Beijing, 100089,  
11   China

12   <sup>3</sup> State Key Laboratory of Remote Sensing Science, Institute of Remote Sensing and Digital  
13   Earth, Chinese Academy of Sciences, Beijing, 100101, China

14   <sup>4</sup> Key Laboratory of Land Surface Pattern and Simulation, Institute of Geographic Sciences  
15   and Natural Resources Research, Chinese Academy of Sciences, Beijing 100101, China

16   <sup>5</sup> College of Resources and Environment, University of Chinese Academy of Sciences,  
17   Beijing 100049, China

18   <sup>6</sup> School of Marine Technology and Geomatics, Jiangsu Ocean University, Lianyungang  
19   222000, China

20  
21   # Runmei Ma, Jie Ban and Qing Wang are the co-first authors.

22   \* Corresponding author: E-mail: [litian@nieh.chinacdc.cn](mailto:litian@nieh.chinacdc.cn)

23 **Abstract**

24 The health risks of fine particulate matter (PM<sub>2.5</sub>) and ambient ozone (O<sub>3</sub>) have been  
25 widely recognized in recent years. An accurate estimate of PM<sub>2.5</sub> and O<sub>3</sub> exposures is  
26 important for supporting health risk analysis and environmental policy-making. The  
27 aim of our study was to construct random forest models with high-performance, and  
28 estimate daily average PM<sub>2.5</sub> concentration and O<sub>3</sub> daily maximum of 8h-average  
29 concentration (O<sub>3</sub>-8hmax) of China in 2005-2017 at a spatial resolution of 1km×1km.  
30 The model variables included meteorological variables, satellite data, chemical  
31 transport model output, geographic variables and socioeconomic variables. Random  
32 forest model based on ten-fold cross validation was established, and spatial and  
33 temporal validations were performed to evaluate the model performance. According  
34 to our sample-based division method, the daily, monthly and yearly estimations of  
35 PM<sub>2.5</sub> from test datasets gave average model fitting R<sup>2</sup> values of 0.85, 0.88 and 0.90,  
36 respectively; these R<sup>2</sup> values were 0.77, 0.77, and 0.69 for O<sub>3</sub>-8hmax, respectively.  
37 The meteorological variables and their lagged values can significantly affect both  
38 PM<sub>2.5</sub> and O<sub>3</sub>-8hmax estimations. During 2005-2017, PM<sub>2.5</sub> exhibited an overall  
39 downward trend, while ambient O<sub>3</sub> experienced an upward trend. Whilst the spatial  
40 patterns of PM<sub>2.5</sub> and O<sub>3</sub>-8hmax barely changed between 2005 and 2017, the temporal  
41 trend had spatial characteristic. The dataset is accessible to the public at  
42 <https://doi.org/10.5281/zenodo.4009308> (Ma et al., 2021), and the shared data set of  
43 Chinese Environmental Public Health Tracking: CEPHT  
44 (<https://cepht.niehs.cn:8282/developSDS3.html>).

45 **1 Introduction**

46 Air pollution is becoming a main concern of modern society due to various health  
47 risks. According to the latest Global Burden of Disease (GBD) report, air pollution  
48 has caused approximately 6.67 million deaths (95% UI: 5.90-7.49 million), and  
49 ranked fourth on the global list of death-related risk factors in 2019 (Health Effects  
50 Institute, 2020; Murray et al., 2020). Ambient fine particulate matter (PM<sub>2.5</sub>) and  
51 ambient ozone (O<sub>3</sub>) have been identified and proven to be related to many health  
52 outcomes. China is known to be one of the countries with the most serious air  
53 pollution in the world. Strict pollution control measures (including *the Air Pollution*  
54 *Prevention and Control Action Plan* and *three-year action plan to fight air pollution*)  
55 were enacted by the Chinese government to control and reduce air pollution since  
56 2013. The implementation of these measures has resulted in a markable drop of  
57 emissions and PM<sub>2.5</sub> concentration. However, the occasional pollution events, as well  
58 as the short development history of air quality monitoring network, have brought  
59 many difficulties to accurately capture the temporal and spatial patterns of PM<sub>2.5</sub> and  
60 O<sub>3</sub> concentrations. Therefore, it is difficult to develop a complete decision-making  
61 basis for handling air pollution. In addition, there are gaps in epidemiological studies  
62 linking air pollutants to health outcomes, due to the lack of accurate measurements of  
63 PM<sub>2.5</sub> and ambient O<sub>3</sub> concentrations. To this end, an accurate estimate of PM<sub>2.5</sub> and  
64 O<sub>3</sub> exposures is essential to support health risk analysis and environmental  
65 policy-making.

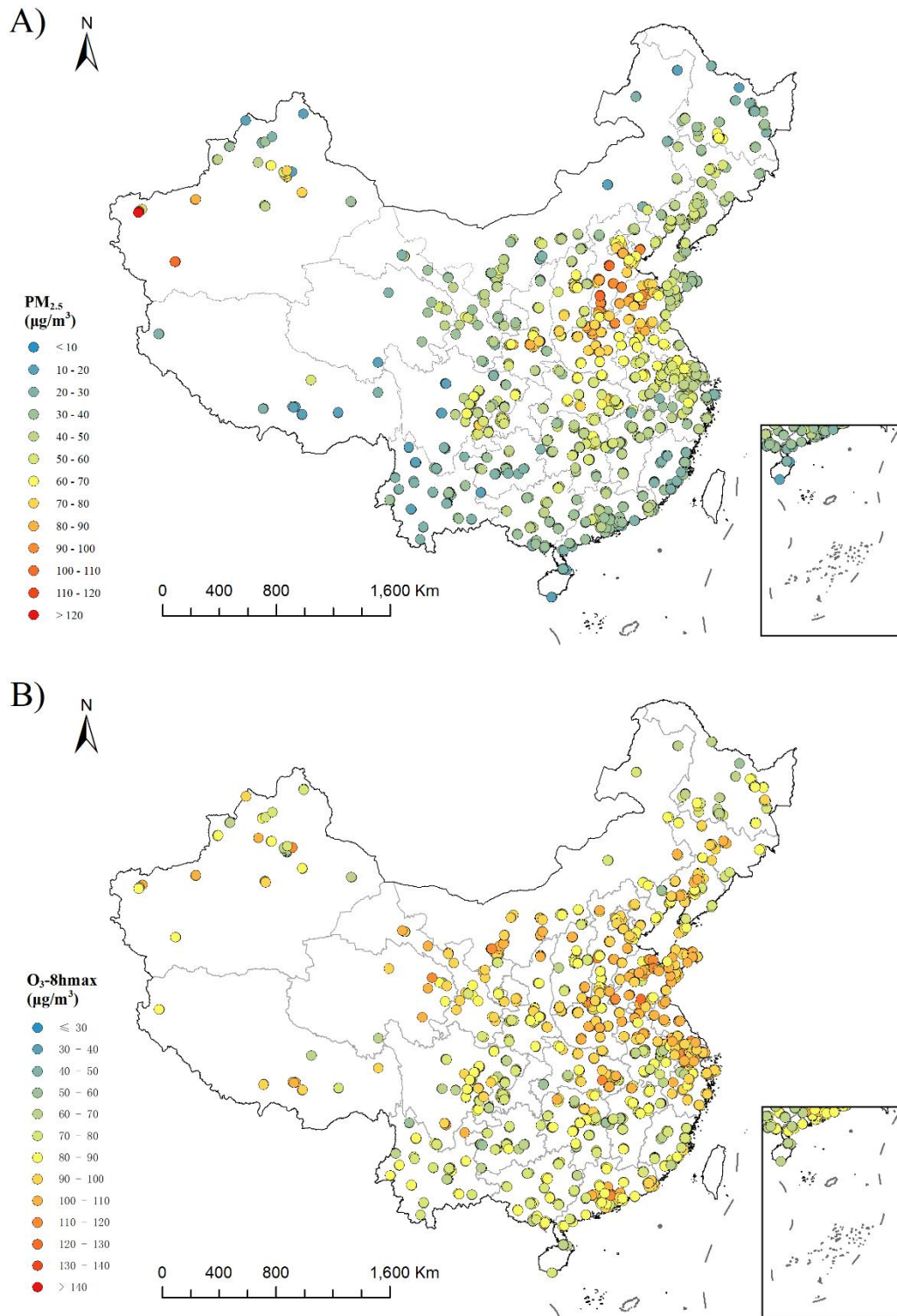
66

67 Suitable model variables and advanced estimation method are important to achieve  
68 accurate modeling. Basically, PM<sub>2.5</sub> is jointly affected by both natural conditions and  
69 human activities over space and time, e.g., Aerosol Optical Depth (AOD),  
70 meteorological conditions, geographic factors and human-related features (Wei et al.,  
71 2021). While O<sub>3</sub> is a secondary pollutant, which is produced by a series of complex  
72 photochemical reactions on the basis of precursor including nitrogen oxides (NO<sub>x</sub>)  
73 and volatile organic compounds (VOCs) under the action of high temperature and  
74 strong radiation. These complex characteristic puts forward higher requirements on  
75 the ability of the modeling method to handle multi-variable, and capture the  
76 non-linear relationships between variables and air pollutants. Many models have been  
77 developed to estimate the spatiotemporal distribution of PM<sub>2.5</sub> and O<sub>3</sub> concentrations  
78 in China. Machine-learning approaches (e.g., random forest (RF), extreme gradient  
79 boosting and deep belief network models) can mine useful information from a large  
80 amount of input data and explore the nonlinear relationship, bring a better  
81 performance in modeling work (Chen et al., 2018, 2019; Di et al., 2017; Li et al.,  
82 2017; Wei et al., 2019; Zhan et al., 2018). However, most of these estimation datasets  
83 cannot balance long time series and high spatiotemporal resolution. Besides, there is  
84 no long-term estimation dataset for both PM<sub>2.5</sub> and O<sub>3</sub> concentrations with high  
85 temporal and spatial resolution for supporting epidemiological research. Therefore, by  
86 incorporating multi-source data into random forest models, this study makes an  
87 attempt to estimate the high-resolution (1km×1km) ambient PM<sub>2.5</sub> and O<sub>3</sub>  
88 concentrations of China in 2005-2017.

89

## 90 **2. Method**

91 The model variables of this study include meteorological variables, geographical  
92 variables, socio-economic variables, satellite data and chemical transport model  
93 output in 2013-2017. Daily average  $PM_{2.5}$  and  $O_3$  daily maximum of 8h-average  
94 concentration ( $O_3$ -8hmax) monitoring data of 1479 sites in 2013-2017 was obtained  
95 (Fig. 1; Fig. S1 and Fig. S2). A  $1km \times 1km$  standard grid is created across the country  
96 ( $35.55^\circ$  N to  $43.12^\circ$  N, and  $112.95^\circ$  E to  $120.35^\circ$  E) with a total of 9495025 grid cells.  
97 The coordinate system of the grid is WGS-84; and the projection of the grid is the  
98 Albers Conical Equal Area Projection. We construct high-performance random forest  
99 (RF) models (temporal resolution: daily; spatial resolution:  $1km \times 1km$ ), and estimate  
100 the grid daily average  $PM_{2.5}$  concentration and  $O_3$ -8hmax concentration of China in  
101 2005-2017.



102

103 **Fig.1 Station distribution in China and average ground monitoring concentration based on**  
 104 **the available data of PM<sub>2.5</sub> (A) and O<sub>3</sub>-8hmax (B) from 2013 to 2017**

105

106 **2.1 Data set**

107 The model variables used in this study mainly include Aqua AOD for PM<sub>2.5</sub> modeling,  
108 GEOS-Chem chemical transport model output for O<sub>3</sub> modeling, and some variables  
109 shared by PM<sub>2.5</sub> and O<sub>3</sub>: 13 meteorological variables (includes boundary layer height,  
110 surface pressure, 2 meter dew point temperature, evaporation, albedo, low cloud cover,  
111 medium cloud cover, high cloud cover, total precipitation, 10 meter U wind  
112 component, 10 meter V wind component, 2 meter surface temperature and surface  
113 solar radiation downwards) and its lag 1 and lag 2, geographic and socio-economic  
114 variables, such as Digital Elevation Model (DEM), Normalized Difference Vegetation  
115 Index (NDVI), population, Gross Domestic Product (GDP), road network and dummy  
116 variables (includes season, month, and spatial dummy variables, province). A more  
117 detailed description of the model variables is given in Table S1. The processing  
118 method has been described in detail in our earlier studies (Ma et al., 2021; Zhao et al.,  
119 2019). Briefly, most of the model variables are processed into 1km×1km resolution  
120 based on the standard grid using interpolation methods (such as inverse distance  
121 weighted and bilinear algorithm) in ArcGIS 10.2 and Python 2.7. For example, AOD  
122 is processed by ENVI 5.3+IDL and extracted into standard grid using ArcPy, then the  
123 inverse distance weighted interpolation is carried out to obtain the 1km×1km  
124 resolution data. For the long-term variables, the corresponding monthly and annual  
125 level value is assigned to each day. Subsequent modeling work was carried out based  
126 on the data set that covering monitoring data and all variables.

127

## 128 **2.2 Random forest model**

129 Random forest is an ensemble machine learning method consisting of many  
 130 individual decision trees growing from bagged data and its prediction is a vote result  
 131 of those trees (Breiman, 2001). The RF algorithm primarily integrates learning  
 132 principles, trains several individual learners, and finally forms a strong learner  
 133 through a certain combination strategy; through multiple rounds of training, multiple  
 134 prediction results are obtained, and the final results are obtained after average  
 135 aggregation.

136

137 The random forest models are established using the 10-fold cross validation method.  
 138 First, this method randomly divides the modeling data set into 10 parts; then 9 of them  
 139 are used for modeling, the remaining one is used for estimation and be compared with  
 140 observations. The verification is repeated until every part is predicted. In this way, the  
 141 modeling and verification of estimation are repeated 10 times in total, and the average  
 142 values of the 10 runs is took as the final result, i.e., the CV-R<sup>2</sup>. The formulae of the  
 143 models are as follows:

144

$$145 \quad PM_{2.5ij} = f(METE_{ij}, lag1METE_{ij}, lag2METE_{ij}, AOD_{ij}, LD_j, ROAD_j, NDVI_j, ELE_j, GDP_j, \\ 146 \quad POP_j, SEASON_i, MON_i, PRO_j) \quad (1)$$

$$147 \quad O_{3-8hmaxij} = f(METE_{ij}, lag1METE_{ij}, lag2METE_{ij}, GEOS_{ij}, LD_j, ROAD_j, NDVI_j, ELE_j, \\ 148 \quad GDP_j, POP_j, SEASON_i, MON_i, PRO_j) \quad (2)$$

149

150 where  $PM_{2.5ij}$  and  $O_{3-8hmaxij}$  are the  $PM_{2.5}$  and  $O_{3-8hmax}$  concentrations on day  $i$  in



151 grid cell  $j$ ;  $METE_{i,j}$  is 13 meteorological variables on day  $i$  in grid cell  $j$ , and lag 1  
152  $METE_{i,j}$  and lag2  $METE_{i,j}$  represent corresponding one-day lag and two-day lag  
153 values, respectively;  $GEOS_{i,j}$  and  $AOD_{i,j}$  are the GEOS-Chem model output and AOD  
154 value on day  $i$  in grid cell  $j$ ;  $LD_j$ ,  $ROAD_j$ ,  $NDVI_j$ ,  $ELE_j$ ,  $GDP_j$  and  $POP_j$  are the land  
155 use coverage, length of a variety of roads, NDVI, elevation, GDP and population in  
156 grid cell  $j$ , respectively;  $SEASON_i$ ,  $MON_i$  and  $PRO_j$  are the season and month of day  $i$ ,  
157 and province of grid cell  $j$ , respectively.

158

159 In general, the random forest parameters that need to be adjusted include  $n\_estimators$   
160 (number of decision trees) and the  $max\_depth$  (maximum depth of the trees). Unlike  
161 the previous methods of manually adjusting parameters, the parameters of random  
162 forest were optimized using GridSearchCV, which can realize cross-validated  
163 grid-search over a parameter grid. After GridSearchCV, we set  $max\_depth$  as 36 and  
164  $n\_estimators$  as 200 for  $PM_{2.5}$  modeling. For  $O_3$ -8hmax modeling, we set  $max\_depth$   
165 as 54 and  $n\_estimators$  as 200.

166

### 167 **2.3 Validation method**

168 To comprehensively verify the model performance, we construct the main models  
169 using sample-based division method. Models using spatial-based and temporal-based  
170 division method are further construct to test the model performance in spatial and  
171 temporal scale.

172

173 The data set was randomly divided into training set (90% of the records) and test set  
174 (10% of the records) by using the sample-based division method. We construct the  
175 main model using the training set with a 10-fold cross-validation. Since the data in the  
176 test set is not used in the main model, "true model performance" can be verified. The  
177 coefficient of determination ( $R^2$ ) of main model on test set (test- $R^2$ ), and the  
178 verification indicators of model uncertainty, the root mean square error (RMSE) and  
179 mean absolute error (MAE) are calculated for the  $PM_{2.5}$  and  $O_3$ -8hmax model,  
180 respectively. The monthly and yearly test- $R^2$  are also calculated.

181

182 For the spatial verification, 90% of the monitoring stations are randomly selected. The  
183 monitoring data of these stations is used as the training set, and the monitoring data of  
184 remaining stations is used as the testing set. For the temporal verification, all date in  
185 2013-2017 is randomly divided into nine and one, and the data in these dates is used  
186 as training and test sets, respectively. After that, the test- $R^2$ , RMSE and MAE are  
187 calculated.

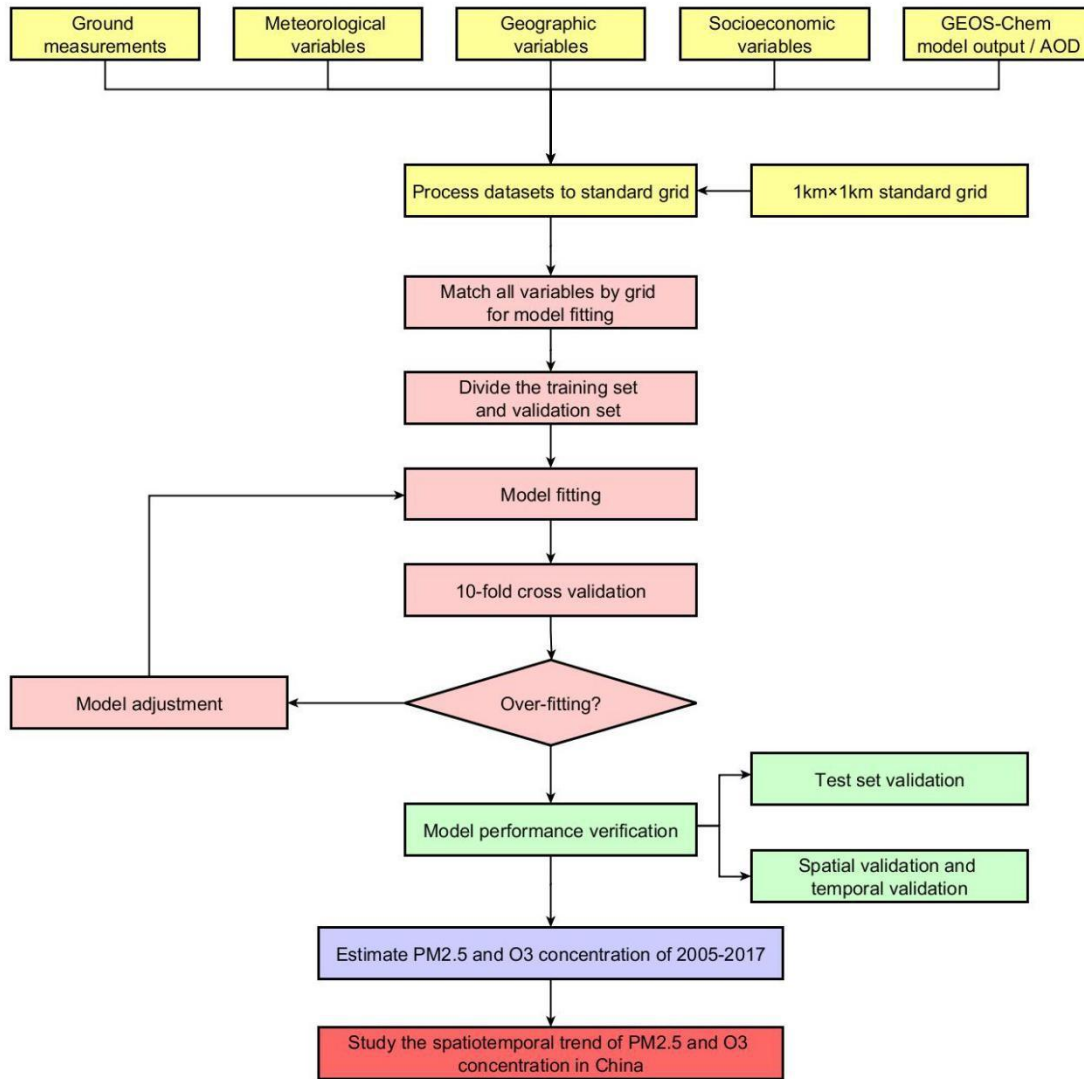
188

#### 189 **2.4 Estimation of daily $PM_{2.5}$ and ambient $O_3$ of China from 2005 to 2017**

190 Based on the final models of  $PM_{2.5}$  and  $O_3$ -8hmax, we estimate the gridded daily  
191 average  $PM_{2.5}$  concentration and  $O_3$ -8hmax concentration of China in 2005-2017. The  
192 spatial pattern and temporal trend of  $PM_{2.5}$  and  $O_3$ -8hmax concentrations are analyzed,  
193 and compared with other modeling products.

194

195 The modeling and estimations are performed in Python 2.7.13 using the  
 196 scikit-learn-0.20.3 and GridSearchCV packages. The workflow of this study is  
 197 displayed in Fig. 2.



198  
 199 **Fig. 2 The workflow of modeling process in the study**

200

### 201 **3 Results and Discussion**

202 A total of 981744 monitoring data records were used in the final model-fitting data set.

203 The mean  $\pm$  standard deviation of PM<sub>2.5</sub> and ambient O<sub>3</sub> concentrations in 2013-2017

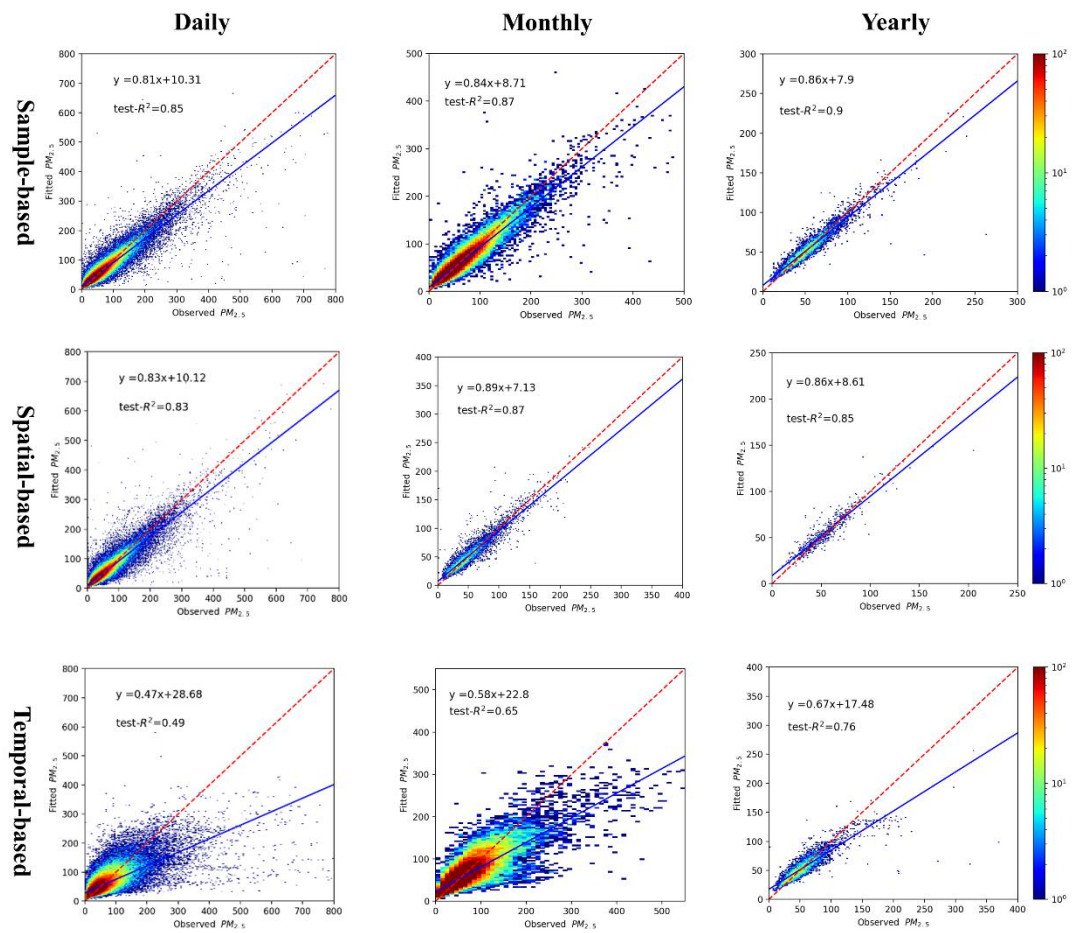
204 were 59.60 $\pm$ 45.85  $\mu\text{g}/\text{m}^3$  and 86.72 $\pm$ 47.73  $\mu\text{g}/\text{m}^3$ , respectively. The results of

205 descriptive analysis for variables included in PM<sub>2.5</sub> and O<sub>3</sub>-8hmax model is shown in  
206 Table S2.

207

### 208 **3.1 Model fitting and validation**

209 The cross-validation results indicate that the estimated PM<sub>2.5</sub> and O<sub>3</sub>-8hmax  
210 concentrations matched reasonably with the observed PM<sub>2.5</sub> and O<sub>3</sub>-8hmax  
211 concentrations, with high fitted test-R<sup>2</sup> values. According to our sample-based  
212 division method, the test-R<sup>2</sup> values of the estimated daily, monthly and yearly PM<sub>2.5</sub>  
213 concentrations were 0.85, 0.88 and 0.90, respectively (Fig. 3). Likewise, the test-R<sup>2</sup>  
214 values of the estimated daily, monthly and yearly O<sub>3</sub>-8hmax concentrations were 0.77,  
215 0.77 and 0.69, respectively (Fig. 4). The RMSE and MAE for PM<sub>2.5</sub> in daily level  
216 were 17.72 and 9.37 µg/m<sup>3</sup>; for O<sub>3</sub>-8hmax, the values were 23.10 and 15.43 µg/m<sup>3</sup>.  
217 The model performance is comparable to previous studies (Di et al., 2017; Li and  
218 Cheng, 2021; Liu et al., 2020; Wei et al., 2021, 2020, 2019). At provincial/city level,  
219 The model performance of PM<sub>2.5</sub> estimations of Shanghai, Beijing, Hubei, Hebei and  
220 Sichuan ranked the top 5 with relatively high test-R<sup>2</sup> (≥0.90), while those of Tibet,  
221 Qinghai, Gansu, Anhui and Yunnan were less accurate with relatively low test-R<sup>2</sup>  
222 values (<0.70). The model performance of O<sub>3</sub>-8hmax estimations of Beijing,  
223 Chongqing, Shanghai, Tianjin and Henan ranked the top 5 with relatively high test-R<sup>2</sup>  
224 values (≥0.83), while those of Gansu, Anhui, Heilongjiang, Guizhou and Tibet were  
225 poorer with relatively low test-R<sup>2</sup> values (<0.62) (Table S3).

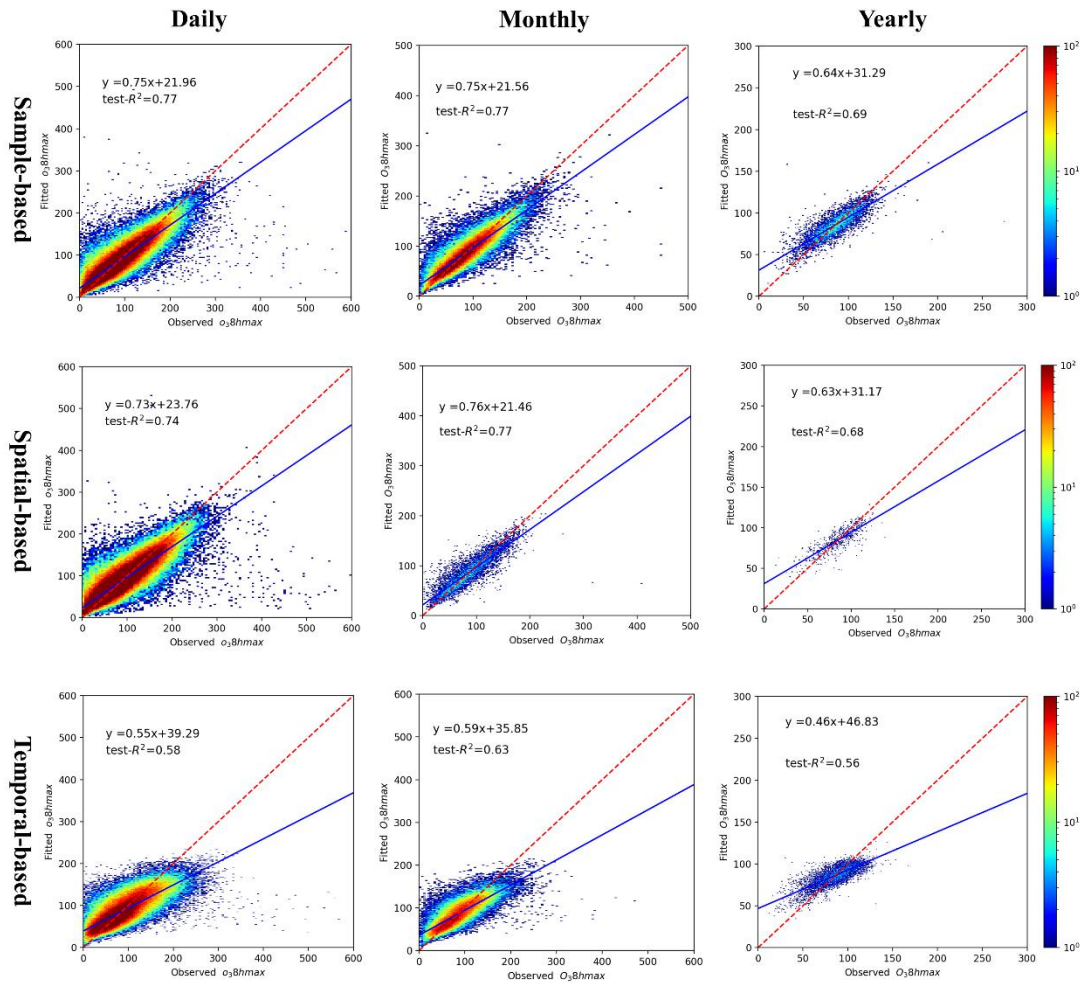


226

227 **Fig. 3 The density plot of PM<sub>2.5</sub> model**

228 From left to right is different temporal scale: daily, monthly and yearly; From top to bottom is

229 different validation method: sample-based, spatial-based and temporal-based.



230

231 **Fig. 4 The density plot of O<sub>3</sub>-8hmax model**

232 From left to right is different temporal scale: daily, monthly and yearly; From top to bottom is  
 233 different validation method: sample-based, spatial-based and temporal-based.

234

235 The spatial and temporal test-R<sup>2</sup> of our models explained the uncertainty to some  
 236 content (Fig. 3 and Fig. 4). The spatial test-R<sup>2</sup> values for daily, monthly and yearly  
 237 PM<sub>2.5</sub> estimation were 0.83, 0.87 and 0.85, respectively; while those of daily, monthly  
 238 and yearly O<sub>3</sub>-8hmax estimations were 0.74, 0.77 and 0.68, respectively. The  
 239 relatively high spatial test-R<sup>2</sup> demonstrates the reasonable performance of our models  
 240 in areas without monitoring stations. The temporal test-R<sup>2</sup> values of daily, monthly  
 241 and yearly PM<sub>2.5</sub> estimations were 0.49, 0.65 and 0.76, respectively; while those of

242 daily, monthly and yearly O<sub>3</sub>-8hmax estimations were 0.58, 0.63 and 0.56,  
243 respectively. These results indicate the uncertainty of our models when modeling data  
244 in historical period, although the performance is among the best compared with  
245 previous studies. The simulation accuracy is a universal issue in the present studies of  
246 air pollutant concentrations in historical period without monitoring data. Further  
247 efforts are need to improve the model performance of historical estimations.

248

### 249 **3.2 Feature importance**

250 The feature importance of the variables in our random forest models is presented in  
251 Table S4-1 and S4-2. Similar to previous studies (Chen et al., 2018; Zhan et al., 2018),  
252 the meteorological factors and their lagged values can significantly affect both PM<sub>2.5</sub>  
253 and O<sub>3</sub>-8hmax modeling. Moreover, the specific features for PM<sub>2.5</sub> and O<sub>3</sub>, AOD and  
254 GEOS-Chem output, also demonstrated high importance in modeling work.

255

256 For PM<sub>2.5</sub> modeling work (Table S4-1), the meteorological variables (boundary layer  
257 height, evaporation, 2 meter dew point temperature) and its lagged effect were among  
258 the top ten important factors, totaling 33.6% in modeling work. The lagged effects  
259 greatly contributed to PM<sub>2.5</sub> modeling. For example, the lag1 boundary layer height  
260 ranked first (17.2%) in our study, which is similar to previous studies (Zhao et al.,  
261 2019). The interpolated AOD (5.6%), DEM (4.9%) and season (3.7%) also  
262 demonstrated high importance, which showed crucial effects of satellite data, terrain  
263 distribution characteristics in the study area, and study period on PM<sub>2.5</sub> modeling. The

264 relative contribution of land-use, NDVI, population density, road length and GDP are  
265 negligible (the importance scores less than 1%). Unlike DEM, these factors are  
266 subjected to the influence of socioeconomic status in study area. In the future study,  
267 the integration of these factors with a higher temporal resolution might change its  
268 contribution to the estimation.

269

270 The feature importance of ambient O<sub>3</sub> is consistent with its formation and dissipation  
271 mechanism: surface solar radiation downwards and its lagged effect according for  
272 39.2% in modeling work (Table S4-2). Other meteorological factors (2 meter  
273 temperature, boundary layer height, 10 meter V wind component, and low cloud cover)  
274 according for totaling 9.54% importance scores. Our analysis also suggests the high  
275 importance of GEOS-Chem model (7.2%), altitude (1.9%), and dummy factors  
276 including year (2.2%) and province (1.6%) in O<sub>3</sub> modeling. By contrast, the relative  
277 contribution of land-use, NDVI and road length are negligible (the importance scores  
278 less than 1%). The high importance rank of population and GDP might be attributed  
279 to the relatively high sensitivity of O<sub>3</sub> to anthropogenic emission sources (compared  
280 to PM<sub>2.5</sub>).

281

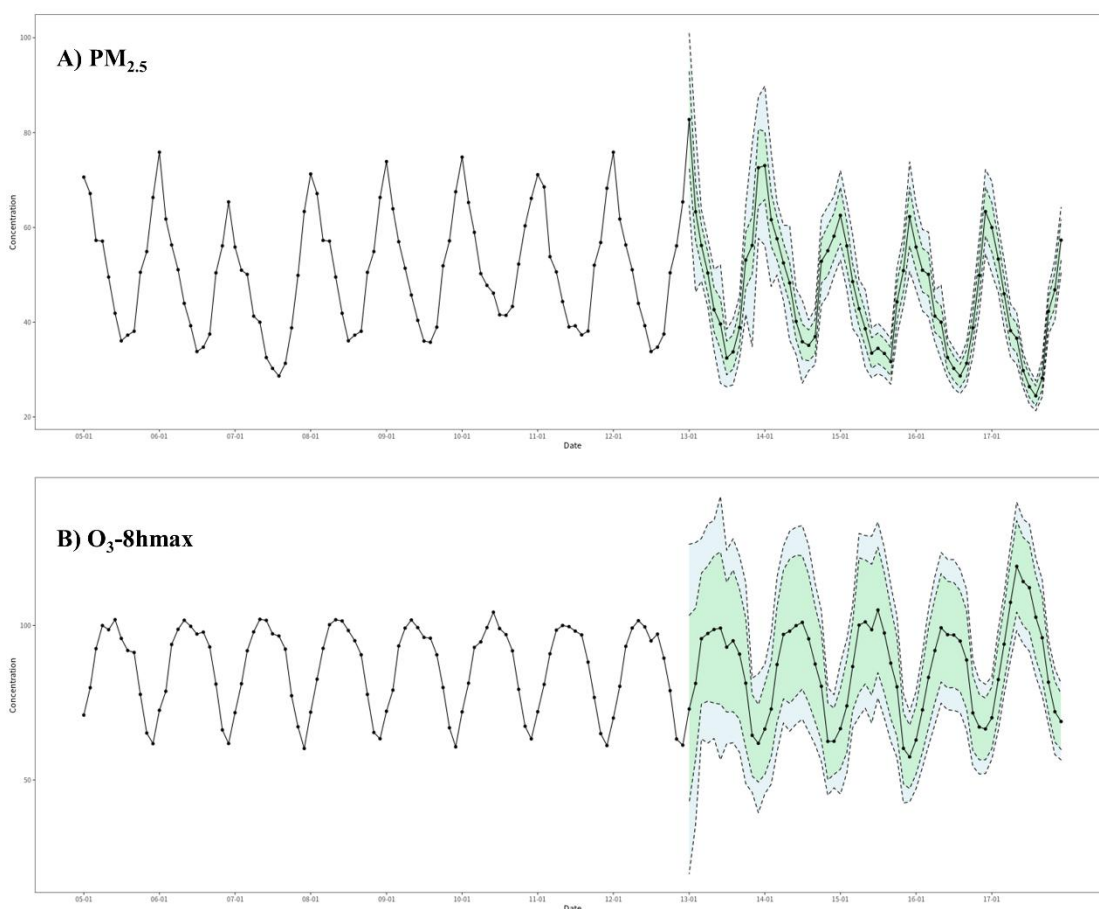
### 282 **3.3 The spatial characteristics and temporal trend of PM<sub>2.5</sub> and ambient O<sub>3</sub> of**

#### 283 **China from 2005 to 2017**

284 During 2005-2017, PM<sub>2.5</sub> showed an overall downward trend, while ambient O<sub>3</sub>  
285 showed an upward trend in recent years (Fig. 5, Fig. S3-S6). Relative to 2005, PM<sub>2.5</sub>



286 concentration has increased by  $2.60 \mu\text{g}/\text{m}^3$  in 2013. Nevertheless, after the  
287 implementation of the *Air Pollution Prevention and Control Action Plan*, a strict  
288 pollution control measure,  $\text{PM}_{2.5}$  concentration has declined by  $11.041 \mu\text{g}/\text{m}^3$  in 2017  
289 (relative to 2013). This has resulted in a downward trend of  $\text{PM}_{2.5}$  concentration in  
290 2005-2017:  $\text{PM}_{2.5}$  concentration in 2017 has decreased by  $8.44 \mu\text{g}/\text{m}^3$  relative to 2005  
291 (Fig. 5 and Fig. S3). In key pollution areas, with the implementation of various air  
292 pollution prevention and control policies,  $\text{PM}_{2.5}$  levels in the Beijing-Tianjin-Hebei  
293 region have dropped the most, but the overall concentration levels are still higher than  
294 those in the Yangtze River Delta and Pearl River Delta (Fig. S4). For  $\text{O}_3$ -8hmax,  
295 upward barely changed. Relative to 2005,  $\text{O}_3$ -8hmax concentrations in 2013 and 2017  
296 have increased by  $0.39 \mu\text{g}/\text{m}^3$  and  $7.83 \mu\text{g}/\text{m}^3$ , respectively. The upward trend during  
297 2005-2017 was mostly due to the significant changes between 2013 and 2017: relative  
298 to 2013, the  $\text{O}_3$ -8hmax concentration has increased by  $7.44 \mu\text{g}/\text{m}^3$  in 2017 (Fig. 5 and  
299 Fig. S5). The Beijing-Tianjin-Hebei region has shown an obvious upward trend since  
300 2013; while the Pearl River Delta region change trend is not obvious (Fig. S6). During  
301 the strict pollution control period, VOC emissions were not effectively controlled  
302 could be one of the main reasons. Therefore, integrated management of VOCs and  
303  $\text{NO}_x$  in key industries and areas is important.



304

305 **Fig.5 The temporal trend of PM<sub>2.5</sub> and O<sub>3</sub>-8hmax concentration in China from 2005-2017**

306 The black dots represent the monthly average PM<sub>2.5</sub> and O<sub>3</sub>-8hmax concentration from 2005 to

307 2017, the blue color band represents the range of the monthly average PM<sub>2.5</sub> and O<sub>3</sub>-8hmax

308 concentration plus or minus the RMSE value from 2013-2017 (period with monitoring data), and

309 the green color band represents the range of the monthly average PM<sub>2.5</sub> and O<sub>3</sub>-8hmax

310 concentration plus or minus the MAE value from 2013-2017 years.

311

312 The seasonal distributions of PM<sub>2.5</sub> and O<sub>3</sub>-8hmax concentrations were obvious

313 during 2005-2017 (Fig. S7 and Fig. S8). The lowest seasonal PM<sub>2.5</sub> concentration

314 occurred in summer, with an average concentration of  $33.6 \pm 11.39 \mu\text{g}/\text{m}^3$ ; and the

315 highest seasonal PM<sub>2.5</sub> concentration occurred in winter, with an average

316 concentration of  $57.4 \pm 21.76 \mu\text{g}/\text{m}^3$ . In winter, temperature inversion occurs frequently,

317 and the thickness of the mixed layer is low, which is not conducive to the diffusion of

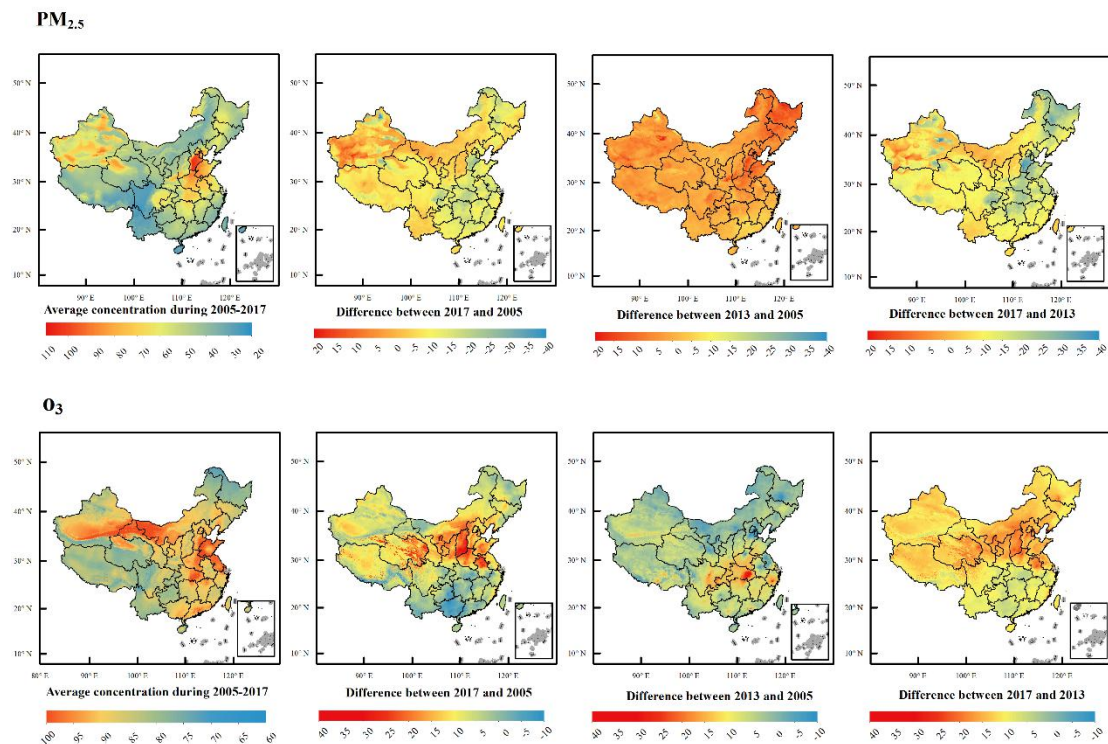
318 pollutants, which leads to the accumulation of PM<sub>2.5</sub> near the ground (Sun et al, 2014).

319 In opposite, the lowest seasonal O<sub>3</sub>-8hmax concentration was in winter, with an  
320 average concentration of 72.65±6.28μg/m<sup>3</sup>; The highest seasonal O<sub>3</sub>-8hmax  
321 concentration was in summer, with an average concentration of 97.44±13.58μg/m<sup>3</sup>.  
322 Temperatures and solar radiation conditions in summer increase the incidence of  
323 severe O<sub>3</sub> pollution events, which is consistent with its formation and dissipation  
324 mechanism.

325

326 The PM<sub>2.5</sub> concentrations in Beijing-Tianjin-Hebei, Chengdu-Chongqing and Xinjiang  
327 regions are higher than other regions, followed by the central China. The PM<sub>2.5</sub>  
328 concentrations in the southwestern regions (Yunnan and Tibet) and western part of  
329 Sichuan Province, are the lowest, followed by the inner-north regions and the south  
330 and southeastern regions (Fig. 6, Fig. S3 and Fig. S4; Table S5). The O<sub>3</sub>-8hmax  
331 concentrations in the Bohai Rim, Yangtze River Delta, Pearl River Delta and other  
332 economically developed regions, southern Xinjiang, Inner Mongolia, and northeastern  
333 Gansu are relatively high (Fig. 6, Fig. S5 and Fig.6; Table S5). This spatial pattern  
334 barely changed during 2005-2017 (Fig. S3 and Fig. S5), but the temporal trend  
335 showed spatial characteristic (Fig. 6; Fig. S4 and S6). For PM<sub>2.5</sub> concentration, the  
336 key pollution areas were severely polluted during 2005-2013. The air pollution  
337 control measures of these regions were strict during 2013-2017, thus the decline was  
338 obvious, especially for the Beijing-Tianjin-Hebei region. For O<sub>3</sub>-8hmax concentration,  
339 the growth rate was not obvious (except for the eastern part of Hubei Province) during  
340 2005-2013. However, after 2013, there was a clear upward trend across the country,

341 especially in the northern China.



342  
343 **Fig. 6 Estimated annual mean and difference of PM<sub>2.5</sub> and O<sub>3</sub>-8hmax concentration in China**  
344 **during 2005 to 2017**

345 The first row is maps of PM<sub>2.5</sub> related indicators, and the second row is maps of O<sub>3</sub>-8hmax related  
346 indicators. From left to right are average concentration during 2005-2017, the difference between  
347 2017 and 2005, the difference between 2013 and 2005, and the difference between 2017 and 2013.

348

### 349 **3.4 Evaluation of the PM<sub>2.5</sub> and O<sub>3</sub> concentration products with comparison with** 350 **other products**

351 Our estimation datasets include the PM<sub>2.5</sub> and O<sub>3</sub>-8hmax concentration data of China  
352 in 2005-2017 with a spatial resolution of 1km×1km resolution. With high spatial and  
353 temporal resolutions, our validation results are comparable with other modeling work  
354 (see Table S6). Considering the future application in epidemiological research, our  
355 estimation datasets would be useful: for acute effects studies, the high spatial  
356 resolution would effectively reduce exposure errors; for chronic effects studies,

357 long-term exposure data is essential for the development of cohort studies.  
358  
359 Nevertheless, our estimation datasets also contain some limitations. First, we did not  
360 use emission data in our model limited by coarse resolution. However the newly  
361 published high-resolution emission inventory of China (<http://meicmodel.org/>) may  
362 be utilized in future estimation studies to improve accuracy. Second, our modeling  
363 still has spatial and temporal uncertainties. In areas where monitoring sites are  
364 sparsely distributed, such as western China, it may be difficult to accurately capture  
365 the association between air pollution concentrations and variables. The model  
366 validation of historical period is also limited. Third, the interpolation process of model  
367 features inevitably introduces systematic errors. Therefore, more high-quality and  
368 high-resolution basic data would be needed in the future.

369

#### 370 **4 Data availability**

371 The estimated PM<sub>2.5</sub> and O<sub>3</sub> data are freely accessible at  
372 <https://doi.org/10.5281/zenodo.4009308> (Ma et al., 2021), and the shared data set of  
373 Chinese Environmental Public Health Tracking: CEPHT  
374 (<https://cepht.niehs.cn:8282/developSDS3.html>).

375

#### 376 **5 Conclusions**

377 We constructed random forest models for simulating of daily average PM<sub>2.5</sub> and  
378 O<sub>3</sub>-8hmax concentrations of China during 2005-2017, with referential feature list and

379 comparable model performance. The estimation dataset would be useful for  
380 supporting both long-term and short-term epidemiological studies. The model can be  
381 further used for simulating daily concentrations of longer time period. The key  
382 findings are summarized as follows. First, RF model proved its superiority in our  
383 study and can be further used in the future estimation of air pollutant concentration.  
384 Second, meteorological data is the most sensitive to PM<sub>2.5</sub> and O<sub>3</sub> modeling. For  
385 PM<sub>2.5</sub> modeling work, boundary layer height, evaporation, 2 meter dew point  
386 temperature and its lagged effects showed the highest sensitivity. For O<sub>3</sub> modeling  
387 work, surface solar radiation downwards and its lagged effect were the most sensitive.  
388 Third, PM<sub>2.5</sub> concentration has trended downward in China, and the key polluted areas  
389 during 2005-2013 were effectively controlled during 2013-2017. O<sub>3</sub> concentration has  
390 trended upward in China, especially in the northern China during 2013-2017.

391

### 392 **Author Contribution**

393 Runmei Ma, Jie Ban and Qing Wang: Software, Investigation, Validation, Formal  
394 analysis, Data curation, Writing - original draft. Yayi Zhang: Formal analysis,  
395 Visualization. Yang Yang, Shenshen Li and Wenjiao Shi: Methodology, Writing -  
396 Review & Editing. Tiantian Li: Conceptualization, Methodology, Writing - Review &  
397 Editing.

398

### 399 **Competing Interests**

400 The authors declare that they have no conflict of interest.

401

## 402 **Acknowledgements**

403 This work was funded by grants from National Natural Science Foundation of China  
404 (Grant No. 92043301 and 42071433).

405

## 406 **Reference**

- 407 Breiman, L., 2001. Random forest. *Machine Learning* 45, 5–32.
- 408 Chen, G., Li, S., Knibbs, L.D., Hamm, N.A.S., Cao, W., Li, T., Guo, J., Ren, H.,  
409 Abramson, M.J., Guo, Y., 2018. A machine learning method to estimate  
410 PM<sub>2.5</sub> concentrations across China with remote sensing, meteorological and  
411 land use information. *Science of The Total Environment* 636, 52–60.  
412 <https://doi.org/10.1016/j.scitotenv.2018.04.251>
- 413 Chen, Z.-Y., Zhang, T.-H., Zhang, R., Zhu, Z.-M., Yang, J., Chen, P.-Y., Ou, C.-Q.,  
414 Guo, Y., 2019. Extreme gradient boosting model to estimate PM<sub>2.5</sub>  
415 concentrations with missing-filled satellite data in China. *Atmospheric*  
416 *Environment* 202, 180–189. <https://doi.org/10.1016/j.atmosenv.2019.01.027>
- 417 Di, Q., Rowland, S., Koutrakis, P., Schwartz, J., 2017. A hybrid model for spatially  
418 and temporally resolved ozone exposures in the continental United States.  
419 *Journal of the Air & Waste Management Association* 67, 39–52.  
420 <https://doi.org/10.1080/10962247.2016.1200159>
- 421 Health Effects Institute, 2020. State of Global Air 2020 28.
- 422 Li, T., Cheng, X., 2021. Estimating daily full-coverage surface ozone concentration  
423 using satellite observations and a spatiotemporally embedded deep learning  
424 approach. *International Journal of Applied Earth Observation and*  
425 *Geoinformation* 101, 102356. <https://doi.org/10.1016/j.jag.2021.102356>
- 426 Li, T., Shen, H., Yuan, Q., Zhang, X., Zhang, L., 2017. Estimating Ground-Level PM  
427 <sub>2.5</sub> by Fusing Satellite and Station Observations: A Geo-Intelligent Deep  
428 Learning Approach: Deep Learning for PM<sub>2.5</sub> Estimation. *Geophys. Res. Lett.*  
429 44, 11,985-11,993. <https://doi.org/10.1002/2017GL075710>
- 430 Liu, R., Ma, Z., Liu, Y., Shao, Y., Zhao, W., Bi, J., 2020. Spatiotemporal distributions  
431 of surface ozone levels in China from 2005 to 2017: A machine learning  
432 approach. *Environment International* 142, 105823.  
433 <https://doi.org/10.1016/j.envint.2020.105823>
- 434 Ma, R., Ban, J., Wang, Q., Zhang, Y., Li, T., 2021. Full-coverage 1 km daily ambient  
435 PM<sub>2.5</sub> and O<sub>3</sub> concentrations of China in 2005-2017 based on multi-variable  
436 random forest model.
- 437 Ma, R., Ban, J., Wang, Q., Zhang, Y., Li, T., 2021. Random Forest Model based Fine  
438 Scale Spatiotemporal O<sub>3</sub> Trends in the Beijing-Tianjin-Hebei region in China,

439 2010 to 2017. Environmental Pollution 116635.

440 Murray, C.J.L., Aravkin, A.Y., Zheng, P., Abbafati, C., Abbas, K.M.,  
441 Abbasi-Kangevari, M., Abd-Allah, F., Abdelalim, A., Abdollahi, M.,  
442 Abdollahpour, I., Abegaz, K.H., Abolhassani, H., Aboyans, V., Abreu, L.G.,  
443 Abrigo, M.R.M., Abualhasan, A., Abu-Raddad, L.J., Abushouk, A.I., Adabi,  
444 M., Adekanmbi, V., Adeoye, A.M., Adetokunboh, O.O., Adham, D., Advani,  
445 S.M., Agarwal, G., Aghamir, S.M.K., Agrawal, A., Ahmad, T., Ahmadi, K.,  
446 Ahmadi, M., Ahmadi, H., Ahmed, M.B., Akalu, T.Y., Akinyemi, R.O.,  
447 Akinyemiju, T., Akombi, B., Akunna, C.J., Alahdab, F., Al-Aly, Z., Alam, K.,  
448 Alam, S., Alam, T., Alanezi, F.M., Alanzi, T.M., Alemu, B. wassihun,  
449 Alhabib, K.F., Ali, M., Ali, S., Alicandro, G., Alinia, C., Alipour, V., Alizade,  
450 H., Aljunid, S.M., Alla, F., Allebeck, P., Almasi-Hashiani, A., Al-Mekhlafi,  
451 H.M., Alonso, J., Altirkawi, K.A., Amini-Rarani, M., Amiri, F., Amugsi, D.A.,  
452 Ancuceanu, R., Anderlini, D., Anderson, J.A., Andrei, C.L., Andrei, T., Angus,  
453 C., Anjomshoa, M., Ansari, F., Ansari-Moghaddam, A., Antonazzo, I.C.,  
454 Antonio, C.A.T., Antony, C.M., Antriyandarti, E., Anvari, D., Anwer, R.,  
455 Appiah, S.C.Y., Arabloo, J., Arab-Zozani, M., Ariani, F., Armoon, B., Ärnlov,  
456 J., Arzani, A., Asadi-Aliabadi, M., Asadi-Pooya, A.A., Ashbaugh, C., Assmus,  
457 M., Atafar, Z., Atnafu, D.D., Atout, M.M.W., Ausloos, F., Ausloos, M., Ayala  
458 Quintanilla, B.P., Ayano, G., Ayanore, M.A., Azari, S., Azarian, G., Azene,  
459 Z.N., Badawi, A., Badiye, A.D., Bahrami, M.A., Bakhshaei, M.H., Bakhtiari,  
460 A., Bakkannavar, S.M., Baldasseroni, A., Ball, K., Ballew, S.H., Balzi, D.,  
461 Banach, M., Banerjee, S.K., Bante, A.B., Baraki, A.G., Barker-Collo, S.L.,  
462 Bärnighausen, T.W., Barrero, L.H., Barthelemy, C.M., Barua, L., Basu, S.,  
463 Baune, B.T., Bayati, M., Becker, J.S., Bedi, N., Beghi, E., Béjot, Y., Bell,  
464 M.L., Bennitt, F.B., Bensenor, I.M., Berhe, K., Berman, A.E., Bhagavathula,  
465 A.S., Bhageerathy, R., Bhala, N., Bhandari, D., Bhattacharyya, K., Bhutta,  
466 Z.A., Bijani, A., Bikbov, B., Bin Sayeed, M.S., Biondi, A., Birihane, B.M.,  
467 Bisignano, C., Biswas, R.K., Bitew, H., Bohlouli, S., Bohluli, M.,  
468 Boon-Dooley, A.S., Borges, G., Borzi, A.M., Borzouei, S., Bosetti, C.,  
469 Boufous, S., Braithwaite, D., Breitborde, N.J.K., Breitner, S., Brenner, H.,  
470 Briant, P.S., Briko, A.N., Briko, N.I., Britton, G.B., Bryazka, D., Bumgarner,  
471 B.R., Burkart, K., Burnett, R.T., Burugina Nagaraja, S., Butt, Z.A., Caetano  
472 dos Santos, F.L., Cahill, L.E., Cámara, L.L.A., Campos-Nonato, I.R.,  
473 Cárdenas, R., Carreras, G., Carrero, J.J., Carvalho, F., Castaldelli-Maia, J.M.,  
474 Castañeda-Orjuela, C.A., Castelpietra, G., Castro, F., Causey, K., Cederroth,  
475 C.R., Cercy, K.M., Cerin, E., Chandan, J.S., Chang, K.-L., Charlson, F.J.,  
476 Chattu, V.K., Chaturvedi, S., Cherbuin, N., Chimed-Ochir, O., Cho, D.Y.,  
477 Choi, J.-Y.J., Christensen, H., Chu, D.-T., Chung, M.T., Chung, S.-C.,  
478 Cicuttini, F.M., Ciobanu, L.G., Cirillo, M., Classen, T.K.D., Cohen, A.J.,  
479 Compton, K., Cooper, O.R., Costa, V.M., Cousin, E., Cowden, R.G., Cross,  
480 D.H., Cruz, J.A., Dahlawi, S.M.A., Damasceno, A.A.M., Damiani, G.,  
481 Dandona, L., Dandona, R., Dangel, W.J., Danielsson, A.-K., Dargan, P.I.,  
482 Darwesh, A.M., Daryani, A., Das, J.K., Das Gupta, R., das Neves, J.,



483 Dávila-Cervantes, C.A., Davitoiu, D.V., De Leo, D., Degenhardt, L., DeLang,  
484 M., Dellavalle, R.P., Demeke, F.M., Demoz, G.T., Demsie, D.G.,  
485 Denova-Gutiérrez, E., Dervenis, N., Dhungana, G.P., Dianatinasab, M., Dias  
486 da Silva, D., Diaz, D., Dibaji Forooshani, Z.S., Djalalinia, S., Do, H.T.,  
487 Dokova, K., Dorostkar, F., Doshmangir, L., Driscoll, T.R., Duncan, B.B.,  
488 Duraes, A.R., Eagan, A.W., Edvardsson, D., El Nahas, N., El Sayed, I., El  
489 Tantawi, M., Elbarazi, I., Elgendy, I.Y., El-Jaafary, S.I., Elyazar, I.R.,  
490 Emmons-Bell, S., Erskine, H.E., Eskandarieh, S., Esmailnejad, S.,  
491 Esteghamati, A., Estep, K., Etemadi, A., Etisso, A.E., Fanzo, J., Farahmand,  
492 M., Fareed, M., Faridnia, R., Farioli, A., Faro, A., Faruque, M., Farzadfar, F.,  
493 Fattahi, N., Fazlzadeh, M., Feigin, V.L., Feldman, R., Fereshtehnejad, S.-M.,  
494 Fernandes, E., Ferrara, G., Ferrari, A.J., Ferreira, M.L., Filip, I., Fischer, F.,  
495 Fisher, J.L., Flor, L.S., Foigt, N.A., Folayan, M.O., Fomenkov, A.A., Force,  
496 L.M., Foroutan, M., Franklin, R.C., Freitas, M., Fu, W., Fukumoto, T.,  
497 Furtado, J.M., Gad, M.M., Gakidou, E., Gallus, S., Garcia-Basteiro, A.L.,  
498 Gardner, W.M., Geberemariam, B.S., Gebreslassie, A.A.A.A., Geremew, A.,  
499 Gershberg Hayoon, A., Gething, P.W., Ghadimi, M., Ghadiri, K., Ghaffarifar,  
500 F., Ghafourifard, M., Ghamari, F., Ghashghaee, A., Ghiasvand, H., Ghith, N.,  
501 Gholamian, A., Ghosh, R., Gill, P.S., Ginindza, T.G.G., Giussani, G.,  
502 Gnedovskaya, E.V., Goharinezhad, S., Gopalani, S.V., Gorini, G., Goudarzi,  
503 H., Goulart, A.C., Greaves, F., Grivna, M., Grosso, G., Gubari, M.I.M.,  
504 Gugnani, H.C., Guimarães, R.A., Guled, R.A., Guo, G., Guo, Y., Gupta, R.,  
505 Gupta, T., Haddock, B., Hafezi-Nejad, N., Hafiz, A., Haj-Mirzaian, Arvin,  
506 Haj-Mirzaian, Arya, Hall, B.J., Halvaei, I., Hamadeh, R.R., Hamidi, S.,  
507 Hammer, M.S., Hankey, G.J., Haririan, H., Haro, J.M., Hasaballah, A.I.,  
508 Hasan, M.M., Hasanpoor, E., Hashi, A., Hassanipour, S., Hassankhani, H.,  
509 Havmoeller, R.J., Hay, S.I., Hayat, K., Heidari, G., Heidari-Soureshjani, R.,  
510 Henrikson, H.J., Herbert, M.E., Herteliu, C., Heydarpour, F., Hird, T.R., Hoek,  
511 H.W., Holla, R., Hoogar, P., Hosgood, H.D., Hossain, N., Hosseini, M.,  
512 Hosseinzadeh, M., Hostiuc, M., Hostiuc, S., Househ, M., Hsairi, M., Hsieh,  
513 V.C., Hu, G., Hu, K., Huda, T.M., Humayun, A., Huynh, C.K., Hwang, B.-F.,  
514 Iannucci, V.C., Ibitoye, S.E., Ikeda, N., Ikuta, K.S., Ilesanmi, O.S., Ilic, I.M.,  
515 Ilic, M.D., Inbaraj, L.R., Ippolito, H., Iqbal, U., Irvani, S.S.N., Irvine, C.M.S.,  
516 Islam, M.M., Islam, S.M.S., Iso, H., Ivers, R.Q., Iwu, C.C.D., Iwu, C.J., Iyamu,  
517 I.O., Jaafari, J., Jacobsen, K.H., Jafari, H., Jafarinia, M., Jahani, M.A.,  
518 Jakovljevic, M., Jalilian, F., James, S.L., Janjani, H., Javaheri, T., Javidnia, J.,  
519 Jeemon, P., Jenabi, E., Jha, R.P., Jha, V., Ji, J.S., Johansson, L., John, O.,  
520 John-Akinola, Y.O., Johnson, C.O., Jonas, J.B., Joukar, F., Jozwiak, J.J.,  
521 Jürisson, M., Kabir, A., Kabir, Z., Kalani, H., Kalani, R., Kalankesh, L.R.,  
522 Kalhor, R., Kanchan, T., Kapoor, N., Karami Matin, B., Karch, A., Karim,  
523 M.A., Kassa, G.M., Katikireddi, S.V., Kayode, G.A., Kazemi Karyani, A.,  
524 Keiyoro, P.N., Keller, C., Kemmer, L., Kendrick, P.J., Khalid, N.,  
525 Khammarnia, M., Khan, E.A., Khan, M., Khatab, K., Khater, M.M., Khatib,  
526 M.N., Khayamzadeh, M., Khazaei, S., Kieling, C., Kim, Y.J., Kimokoti, R.W.,

527 Kisa, A., Kisa, S., Kivimäki, M., Knibbs, L.D., Knudsen, A.K.S., Kocarnik,  
 528 J.M., Kochhar, S., Kopec, J.A., Korshunov, V.A., Koul, P.A., Koyanagi, A.,  
 529 Kraemer, M.U.G., Krishan, K., Krohn, K.J., Kromhout, H., Kuate Defo, B.,  
 530 Kumar, G.A., Kumar, V., Kurmi, O.P., Kusuma, D., La Vecchia, C., Lacey, B.,  
 531 Lal, D.K., Laloo, R., Lallukka, T., Lami, F.H., Landires, I., Lang, J.J., Langan,  
 532 S.M., Larsson, A.O., Lasrado, S., Lauriola, P., Lazarus, J.V., Lee, P.H., Lee,  
 533 S.W.H., LeGrand, K.E., Leigh, J., Leonardi, M., Lescinsky, H., Leung, J.,  
 534 Levi, M., Li, S., Lim, L.-L., Linn, S., Liu, Shiwei, Liu, Simin, Liu, Y., Lo, J.,  
 535 Lopez, A.D., Lopez, J.C.F., Lopukhov, P.D., Lorkowski, S., Lotufo, P.A., Lu,  
 536 A., Lugo, A., Maddison, E.R., Mahasha, P.W., Mahdavi, M.M., Mahmoudi,  
 537 M., Majeed, A., Maleki, A., Maleki, S., Malekzadeh, R., Malta, D.C., Mamun,  
 538 A.A., Manda, A.L., Manguerra, H., Mansour-Ghanaei, F., Mansouri, B.,  
 539 Mansournia, M.A., Mantilla Herrera, A.M., Maravilla, J.C., Marks, A., Martin,  
 540 R.V., Martini, S., Martins-Melo, F.R., Masaka, A., Masoumi, S.Z., Mathur,  
 541 M.R., Matsushita, K., Maulik, P.K., McAlinden, C., McGrath, J.J., McKee, M.,  
 542 Mehndiratta, M.M., Mehri, F., Mehta, K.M., Memish, Z.A., Mendoza, W.,  
 543 Menezes, R.G., Mengesha, E.W., Mereke, A., Mereta, S.T., Meretoja, A.,  
 544 Meretoja, T.J., Mestrovic, T., Miazgowski, B., Miazgowski, T., Michalek,  
 545 I.M., Miller, T.R., Mills, E.J., Mini, G., Miri, M., Mirica, A., Mirrakhimov,  
 546 E.M., Mirzaei, H., Mirzaei, M., Mirzaei, R., Mirzaei-Alavijeh, M., Misganaw,  
 547 A.T., Mithra, P., Moazen, B., Mohammad, D.K., Mohammad, Y., Mohammad  
 548 Gholi Mezerji, N., Mohammadian-Hafshejani, A., Mohammadifard, N.,  
 549 Mohammadpourhodki, R., Mohammed, A.S., Mohammed, H., Mohammed,  
 550 J.A., Mohammed, S., Mokdad, A.H., Molokhia, M., Monasta, L., Mooney,  
 551 M.D., Moradi, G., Moradi, M., Moradi-Lakeh, M., Moradzadeh, R., Moraga,  
 552 P., Morawska, L., Morgado-da-Costa, J., Morrison, S.D., Mosapour, A.,  
 553 Mosser, J.F., Mouodi, S., Mousavi, S.M., Mousavi Khaneghah, A., Mueller,  
 554 U.O., Mukhopadhyay, S., Mullany, E.C., Musa, K.I., Muthupandian, S.,  
 555 Nabhan, A.F., Naderi, M., Nagarajan, A.J., Nagel, G., Naghavi, M.,  
 556 Naghshtabrizi, B., Naimzada, M.D., Najafi, F., Nangia, V., Nansseu, J.R.,  
 557 Naserbakht, M., Nayak, V.C., Negoi, I., Ngunjiri, J.W., Nguyen, C.T., Nguyen,  
 558 H.L.T., Nguyen, M., Nigatu, Y.T., Nikbakhsh, R., Nixon, M.R., Nnaji, C.A.,  
 559 Nomura, S., Norrving, B., Noubiap, J.J., Nowak, C., Nunez-Samudio, V.,  
 560 Oțoiu, A., Oancea, B., Odell, C.M., Ogbo, F.A., Oh, I.-H., Okunga, E.W.,  
 561 Oladnabi, M., Olagunju, A.T., Olusanya, B.O., Olusanya, J.O., Omer, M.O.,  
 562 Ong, K.L., Onwujekwe, O.E., Orpana, H.M., Ortiz, A., Osarenotor, O., Osei,  
 563 F.B., Ostroff, S.M., Otstavnov, N., Otstavnov, S.S., Øverland, S., Owolabi,  
 564 M.O., P A, M., Padubidri, J.R., Palladino, R., Panda-Jonas, S., Pandey, A.,  
 565 Parry, C.D.H., Pasovic, M., Pasupula, D.K., Patel, S.K., Pathak, M., Patten,  
 566 S.B., Patton, G.C., Pazoki Toroudi, H., Peden, A.E., Pennini, A., Pepito,  
 567 V.C.F., Peprah, E.K., Pereira, D.M., Pesudovs, K., Pham, H.Q., Phillips, M.R.,  
 568 Piccinelli, C., Pilz, T.M., Piradov, M.A., Pirsahab, M., Plass, D., Polinder, S.,  
 569 Polkinghorne, K.R., Pond, C.D., Postma, M.J., Pourjafar, H., Pourmalek, F.,  
 570 Poznańska, A., Prada, S.I., Prakash, V., Pribadi, D.R.A., Pupillo, E., Quazi

571 Syed, Z., Rabiee, M., Rabiee, N., Radfar, A., Rafiee, A., Raggi, A., Rahman,  
 572 M.A., Rajabpour-Sanati, A., Rajati, F., Rakovac, I., Ram, P., Ramezanzadeh,  
 573 K., Ranabhat, C.L., Rao, P.C., Rao, S.J., Rashedi, V., Rathi, P., Rawaf, D.L.,  
 574 Rawaf, S., Rawal, L., Rawassizadeh, R., Rawat, R., Razo, C., Redford, S.B.,  
 575 Reiner, R.C., Reitsma, M.B., Remuzzi, G., Renjith, V., Renzaho, A.M.N.,  
 576 Resnikoff, S., Rezaei, Negar, Rezaei, Nima, Rezapour, A., Rhinehart, P.-A.,  
 577 Riahi, S.M., Ribeiro, D.C., Ribeiro, D., Rickard, J., Rivera, J.A., Roberts,  
 578 N.L.S., Rodríguez-Ramírez, S., Roeber, L., Ronfani, L., Room, R., Roshandel,  
 579 G., Roth, G.A., Rothenbacher, D., Rubagotti, E., Rwegerera, G.M., Sabour, S.,  
 580 Sachdev, P.S., Saddik, B., Sadeghi, E., Sadeghi, M., Saeedi, R., Saeedi  
 581 Moghaddam, S., Safari, Y., Safi, S., Safiri, S., Sagar, R., Sahebkar, A., Sajadi,  
 582 S.M., Salam, N., Salamati, P., Salem, H., Salem, M.R.R., Salimzadeh, H.,  
 583 Salman, O.M., Salomon, J.A., Samad, Z., Samadi Kafil, H., Sambala, E.Z.,  
 584 Samy, A.M., Sanabria, J., Sánchez-Pimienta, T.G., Santomauro, D.F., Santos,  
 585 I.S., Santos, J.V., Santric-Milicevic, M.M., Saraswathy, S.Y.I.,  
 586 Sarmiento-Suárez, R., Sarrafzadegan, N., Sartorius, B., Sarveazad, A., Sathian,  
 587 B., Sathish, T., Sattin, D., Saxena, S., Schaeffer, L.E., Schiavolin, S., Schlaich,  
 588 M.P., Schmidt, M.I., Schutte, A.E., Schwebel, D.C., Schwendicke, F., Senbeta,  
 589 A.M., Senthilkumaran, S., Sepanlou, S.G., Serdar, B., Serre, M.L., Shadid, J.,  
 590 Shafaat, O., Shahabi, S., Shaheen, A.A., Shaikh, M.A., Shalash, A.S.,  
 591 Shams-Beyranvand, M., Shamsizadeh, M., Sharafi, K., Sheikh, A.,  
 592 Sheikhtaheri, A., Shibuya, K., Shield, K.D., Shigematsu, M., Shin, J.I., Shin,  
 593 M.-J., Shiri, R., Shirkoobi, R., Shuval, K., Siabani, S., Sierpinski, R.,  
 594 Sigfusdottir, I.D., Sigurvinsdottir, R., Silva, J.P., Simpson, K.E., Singh, J.A.,  
 595 Singh, P., Skiadaresi, E., Skou, S.T.S., Skryabin, V.Y., Smith, E.U.R., Soheili,  
 596 A., Soltani, S., Soofi, M., Sorensen, R.J.D., Soriano, J.B., Sorrie, M.B.,  
 597 Soshnikov, S., Soyiri, I.N., Spencer, C.N., Spotin, A., Sreeramareddy, C.T.,  
 598 Srinivasan, V., Stanaway, J.D., Stein, C., Stein, D.J., Steiner, C., Stockfelt, L.,  
 599 Stokes, M.A., Straif, K., Stubbs, J.L., Sufiyan, M.B., Suleria, H.A.R.,  
 600 Suliankatchi Abdulkader, R., Sulo, G., Sultan, I., Szumowski, Ł.,  
 601 Tabarés-Seisdedos, R., Tabb, K.M., Tabuchi, T., Taherkhani, A., Tajdini, M.,  
 602 Takahashi, K., Takala, J.S., Tamiru, A.T., Taveira, N., Tehrani-Banihashemi,  
 603 A., Temsah, M.-H., Tesema, G.A., Tessema, Z.T., Thurston, G.D., Titova,  
 604 M.V., Tohidinik, H.R., Tonelli, M., Topor-Madry, R., Topouzis, F., Torre,  
 605 A.E., Touvier, M., Tovani-Palone, M.R.R., Tran, B.X., Travillian, R.,  
 606 Tsatsakis, A., Tudor Car, L., Tyrovolas, S., Uddin, R., Umeokonkwo, C.D.,  
 607 Unnikrishnan, B., Upadhyay, E., Vacante, M., Valdez, P.R., van Donkelaar,  
 608 A., Vasankari, T.J., Vasseghian, Y., Veisani, Y., Venketasubramanian, N.,  
 609 Violante, F.S., Vlassov, V., Vollset, S.E., Vos, T., Vukovic, R., Waheed, Y.,  
 610 Wallin, M.T., Wang, Y., Wang, Y.-P., Watson, A., Wei, J., Wei, M.Y.W.,  
 611 Weintraub, R.G., Weiss, J., Werdecker, A., West, J.J., Westerman, R.,  
 612 Whisnant, J.L., Whiteford, H.A., Wiens, K.E., Wolfe, C.D.A., Wozniak, S.S.,  
 613 Wu, A.-M., Wu, J., Wulf Hanson, S., Xu, G., Xu, R., Yadgir, S., Yahyazadeh  
 614 Jabbari, S.H., Yamagishi, K., Yaminfirooz, M., Yano, Y., Yaya, S.,

615 Yazdi-Feyzabadi, V., Yeheyis, T.Y., Yilgwan, C.S., Yilma, M.T., Yip, P.,  
616 Yonemoto, N., Younis, M.Z., Younker, T.P., Yousefi, B., Yousefi, Z.,  
617 Yousefinezhadi, T., Yousuf, A.Y., Yu, C., Yusefzadeh, H., Zahirian  
618 Moghadam, T., Zamani, M., Zamanian, M., Zandian, H., Zastrozhin, M.S.,  
619 Zhang, Y., Zhang, Z.-J., Zhao, J.T., Zhao, X.-J.G., Zhao, Y., Zhou, M.,  
620 Ziapour, A., Zimsen, S.R.M., Brauer, M., Afshin, A., Lim, S.S., 2020. Global  
621 burden of 87 risk factors in 204 countries and territories, 1990–2019: a  
622 systematic analysis for the Global Burden of Disease Study 2019. *The Lancet*  
623 396, 1223–1249. [https://doi.org/10.1016/S0140-6736\(20\)30752-2](https://doi.org/10.1016/S0140-6736(20)30752-2)

624 Wei, J., Huang, W., Li, Z., Xue, W., Peng, Y., Sun, L., Cribb, M., 2019. Estimating  
625 1-km-resolution PM<sub>2.5</sub> concentrations across China using the space-time  
626 random forest approach. *Remote Sensing of Environment* 231, 111221.  
627 <https://doi.org/10.1016/j.rse.2019.111221>

628 Wei, J., Li, Z., Cribb, M., Huang, W., Xue, W., Sun, L., Guo, J., Peng, Y., Li, J.,  
629 Lyapustin, A., Liu, L., Wu, H., Song, Y., 2020. Improved 1 km resolution  
630 PM<sub>2.5</sub> estimates across China using enhanced  
631 space–time extremely randomized trees. *Atmos. Chem. Phys.* 20, 3273–3289.  
632 <https://doi.org/10.5194/acp-20-3273-2020>

633 Wei, J., Li, Z., Lyapustin, A., Sun, L., Peng, Y., Xue, W., Su, T., Cribb, M., 2021.  
634 Reconstructing 1-km-resolution high-quality PM<sub>2.5</sub> data records from 2000 to  
635 2018 in China: spatiotemporal variations and policy implications. *Remote*  
636 *Sensing of Environment* 252, 112136.  
637 <https://doi.org/10.1016/j.rse.2020.112136>

638 Zhan, Y., Luo, Y., Deng, X., Grieneisen, M.L., Zhang, M., Di, B., 2018.  
639 Spatiotemporal prediction of daily ambient ozone levels across China using  
640 random forest for human exposure assessment. *Environmental Pollution* 233,  
641 464–473. <https://doi.org/10.1016/j.envpol.2017.10.029>

642 Zhao, C., Wang, Q., Ban, J., Liu, Z., Li, T., 2019. Estimating the daily PM<sub>2.5</sub>  
643 concentration in the Beijing-Tianjin-Hebei region using a random forest model  
644 with a 0.01° × 0.01° spatial resolution. *Environment international* 134,  
645 105297.

646